Journal of
Polymer & Composites
https://journals.stmjournals.com/jopc

ISSN: 2321-2810 (Online)
ISSN: 2321-8525 (Print)
Volume 14, Issue 3, 2026
DOI (Journal): 10.37591/JoPC

Research JoPC

Optimized Utilization of Kota Stone Slurry Waste in Fly Ash–Based Geopolymer Mortar: A Taguchi-Driven Approach

Pawan Patidar[1,*], Pawan Kalla[2], Pravesh Saini[3]

Abstract

The large-scale generation of stone-processing wastes presents a critical sustainability challenge and an opportunity for value-added reuse in construction materials. This study develops a high-performance fly ash geopolymer mortar by partially replacing Class F fly ash with Kota stone slurry waste (KSSW) and optimizing the key mix parameters using a Taguchi design framework. Five governing factors—binder replacement level, NaOH molarity, sodium silicate–to–sodium hydroxide ratio (SS/SH), curing temperature, and alkaline solution-to-binder ratio (A/B)—were systematically optimized using ultrasonic pulse velocity (UPV; larger-the-better) and water absorption (smaller-the-better) as primary compactness and durability indicators, with strength confirmation. The optimum combination (25% KSSW, 12 M NaOH, SS/SH = 1, curing at 60 °C, A/B = 0.5) achieved a UPV of 4380 m/s (+16.7%) and a minimum water absorption of 3.1% (−63.9%) relative to the control, indicating substantial matrix densification. Correspondingly, compressive and flexural strengths reached 25.6 MPa (+143.8%) and 3.95 MPa (+62.6%) at 28 days. Regression modelling and ANOVA confirmed curing temperature as the dominant factor, while excessive activator content adversely affected performance. Durability evaluation of the control and optimum mixes showed progressive degradation under acid exposure, whereas sulphate immersion up to 90 days resulted in net strength gain with early mass increase (pore filling) followed by slight mass loss at longer exposure; drying shrinkage remained comparable between mixes (≈0.00158 at 90 days), indicating no shrinkage penalty for the optimized system. Multi-scale characterization (XRD, SEM–EDS elemental mapping, FTIR, XRF, and TGA/DTG–DSC) supported improved gel development and Ca-assisted densification in the KSSW-modified matrix. Overall, the results establish KSSW as a viable supplementary binder and demonstrate that strength-driven statistical optimization enables a resource-efficient, high-performance geopolymer mortar suitable for sustainable construction applications.

Keywords: Geopolymer mortar; Kota stone slurry waste; Taguchi optimization; Ultrasonic pulse velocity; Water absorption.

***Author for Correspondence**
Pawan Patidar

[1,3]Research Scholar, Department of Civil Engineering, Malaviya National Institute of Technology, Jaipur, Rajasthan, India
[2]Associate Professor, Department of Civil Engineering, Malaviya National Institute of Technology, Jaipur, Rajasthan, India

Received Date: April 16, 2026
Accepted Date: April 28, 2026
Published Date: May 21, 2026

Citation: Pawan Patidar, Pawan Kalla, Pravesh Saini. Optimized Utilization of Kota Stone Slurry Waste in Fly Ash–Based Geopolymer Mortar: A Taguchi-Driven Approach. Journal of Polymer & Composites. 2026; 14(3): 426–445p.

INTRODUCTION

The escalating environmental footprint associated with Ordinary Portland Cement (OPC) production has intensified global efforts to develop sustainable, low-carbon construction materials material [1,2]. In this context, geopolymer binders produced through the alkali activation of aluminosilicate precursors have emerged as a promising alternative owing to their significantly lower CO_2 emissions, superior durability, and adaptability across diverse construction applications [3,4]. Among these systems, geopolymer mortars have gained particular attention for use in masonry, repair works, precast components, and emerging construction technologies [5]. A key driver behind the growing adoption of geopolymer mortars is their ability to incorporate industrial and construction wastes as primary raw materials, thereby reducing landfill disposal while promoting circular-economy practices [4,6]. Fly ash remains one of the most widessssly investigated geopolymer precursors due to its widespread availability, favourable particle morphology, and high amorphous aluminosilicate content [2]. Numerous studies have demonstrated that fly ash-based geopolymer mortars can achieve high mechanical performance and durability when blended with supplementary materials such as ground-granulated blast furnace slag, rice husk ash, calcined clays, ceramic wastes, and bentonite, which enhance geopolymerization kinetics and microstructural compactness [7–10]. Recent advances further highlight the role of mineral additives and nanomaterials in improving long-term durability and functional performance [11,12].

Beyond precursor selection, the chemistry of the alkaline activator system particularly sodium hydroxide concentration and the sodium silicate-to-sodium hydroxide (SS/SH) ratio critically governs dissolution, polycondensation, gel formation, and pore structure in geopolymer mortars [13–15]. Optimized activator compositions promote the formation of dense N–A–S–H and hybrid C-(N)-A–S–H gels, resulting in enhanced strength and durability, whereas excessive alkalinity may adversely affect workability and microstructural [16]. Curing conditions further influence geopolymer performance; elevated temperatures in the range of 60–90 °C have been shown to accelerate reaction kinetics and strength development in fly ash- and waste-based systems, although excessive heating can induce shrinkage cracking and increased permeability [17–19]. Parallel to these material-level challenges, the global dimensional-stone industry generates enormous quantities of waste during quarrying, cutting, sawing, and polishing operations. Large-scale production of granite, marble, limestone, and related stones for flooring and architectural applications is inherently accompanied by substantial waste streams in the form of quarry rejects, off-cuts, and fine sludge [20]. As illustrated in Figure 1, even conservative waste factors of 0.45–0.50 result in tens to hundreds of million tonnes of stone waste annually, with China (~175 Mt y^{-1}) and India (~110 Mt y^{-1}) alone accounting for a dominant share of global generation [21]. This waste not only poses serious land, air, and water pollution concerns, but also represents a largely underutilized calcium and silica-rich resource.

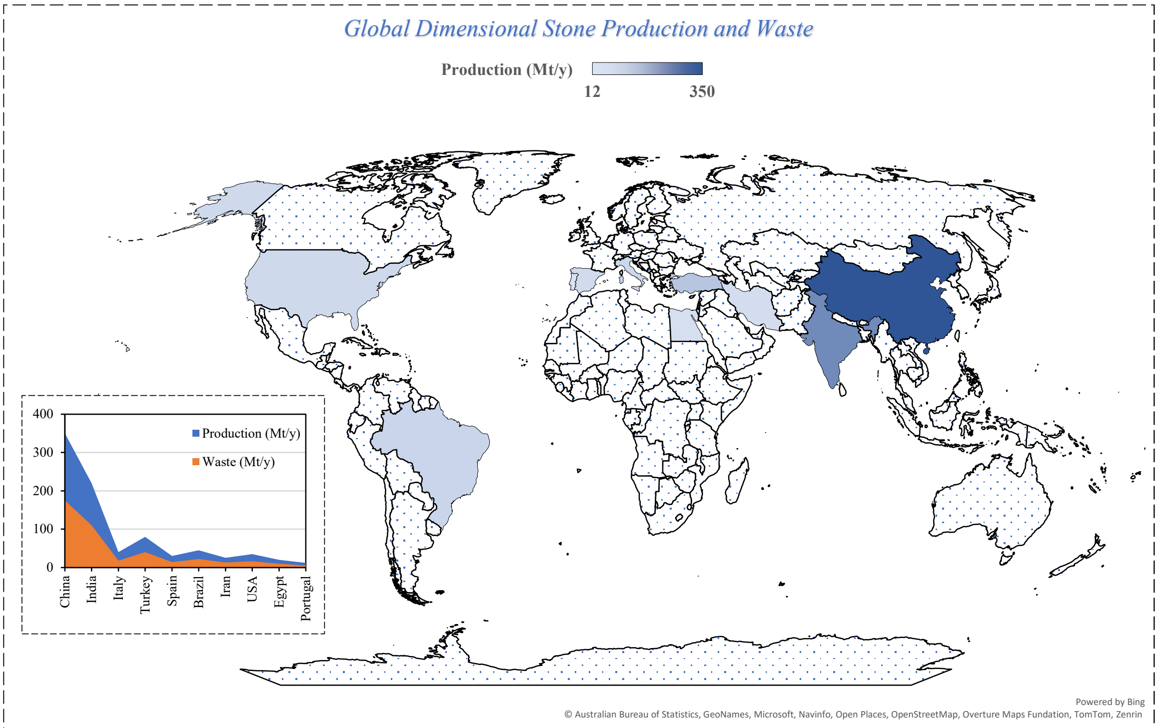

Figure 1. Global dimensional-stone production and waste generation.

Accordingly, the development of high-volume, performance-oriented pathways to upcycle dimensional stone waste into geopolymer mortars is both an environmental necessity and a circular-economy opportunity. In this context, Kota stone slurry waste (KSSW), a limestone-derived by-product abundantly generated in India, offers significant potential as a supplementary binder in fly ash-based geopolymer mortars. However, systematic optimization of mix design parameters and validation of durability-related performance remain limited. Addressing this gap, the present study integrates Taguchi-based experimental optimization with mechanical, durability, and microstructural evaluation to establish an efficient and sustainable route for valorising KSSW in geopolymer mortar applications. The Kota stone industry generates large volumes of waste in the form of solid chips and fine slurry during quarrying, cutting, and polishing operations.

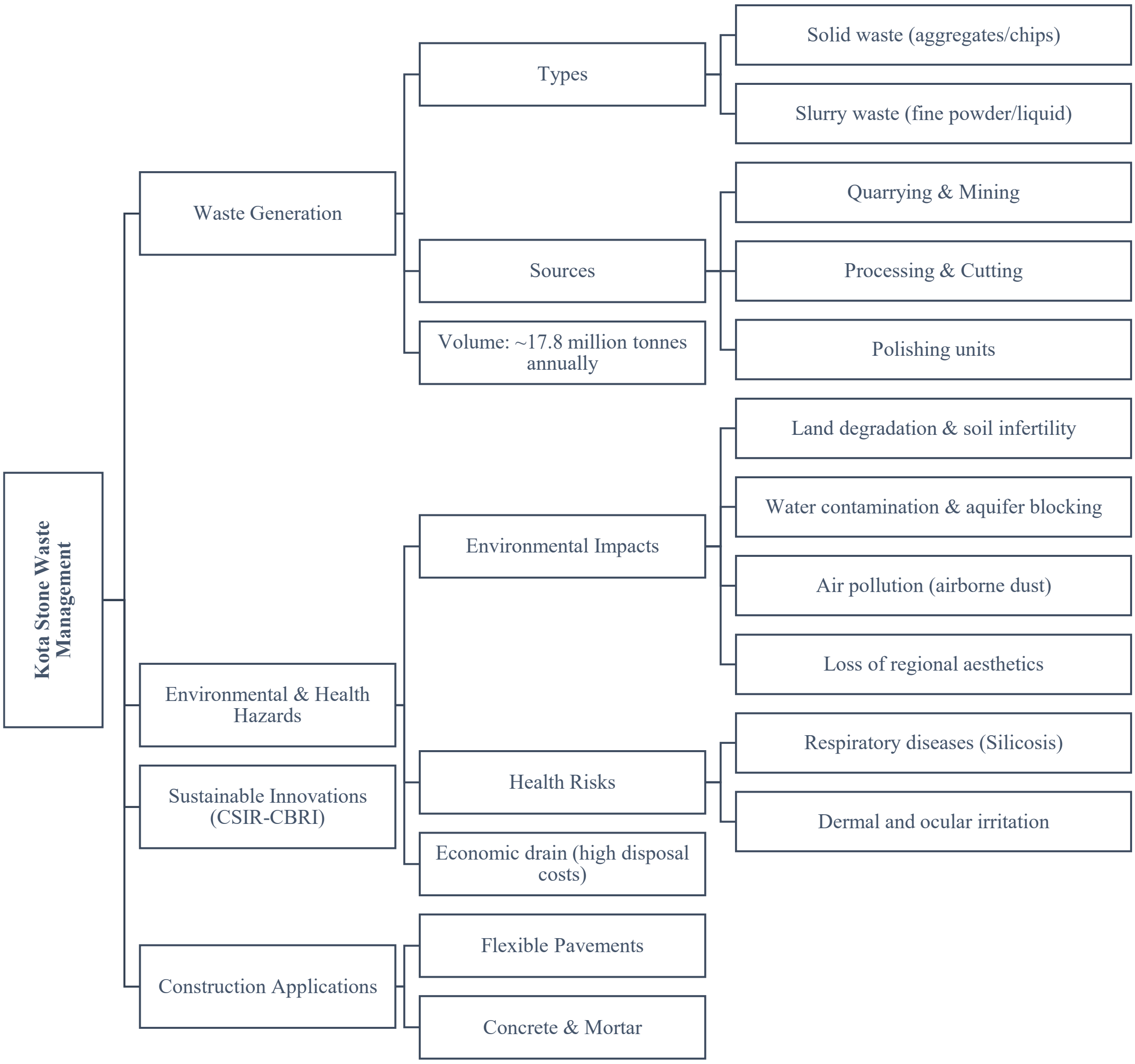

Figure 2. Schematic overview of Kota stone waste generation, sources, environmental and health impacts.

This waste stream, estimated at ~17.8 million tonnes annually, poses serious environmental and health challenges, including land degradation, water contamination, airborne dust, and occupational diseases such as silicosis (See Figure 2). In addition to environmental impacts, improper disposal leads to economic losses due to high handling and landfill costs. Recent sustainability-driven initiatives highlight the need to redirect this waste toward value-added construction applications, particularly in concrete and mortar systems, to mitigate environmental damage while promoting circular economy practices. Despite extensive research on geopolymer mortars, most studies have focused on conventional aluminosilicate precursors, with limited systematic investigation into the valorization of stone-processing wastes such as Kota stone slurry waste (KSSW) as a supplementary binder. Furthermore, geopolymer mix designs are frequently developed using trial-and-error methods, and the coupled effects of critical parameters including binder replacement level, alkaline activator concentration, alkalinity ratio, curing temperature, and alkaline solution-to-binder ratio remain insufficiently optimized using statistically robust frameworks. To address these gaps, the present study employs a Taguchi-based design of experiments to optimize fly ash–KSSW geopolymer mortar, evaluate its fresh and hardened performance, and elucidate the governing mechanisms through mineralogical characterization.

MATERIALS AND METHODS

Fly Ash

Class F fly ash, obtained from the Suratgarh Thermal Power Plant, Rajasthan, India, was used as the primary aluminosilicate precursor in this study. Its suitability for geopolymerization was confirmed through X-ray fluorescence (XRF) analysis (Table 1), which shows a high combined content of SiO_2 and Al_2O_3 (≈89 wt.%) and a low CaO content (≈6 wt.%). This low-calcium composition is characteristic of Class F fly ash and Favors alkali activation through dissolution of amorphous aluminosilicate phases, leading predominantly to N–A–S–H gel formation. The fine particle size and predominantly spherical morphology of fly ash further contribute to improved particle packing and a dense geopolymer matrix, which is essential for durability-related properties such as ultrasonic pulse velocity and water absorption.

Table 1. Oxide composition of fly ash and Kota stone slurry waste determined by XRF analysis (wt.%).

Material	Al_2O_3	CaO	Fe_2O_3	MgO	P_2O_5	K_2O	SiO_2	Na_2O	TiO_2	LOI
Fly Ash	31.56	5.89	3.26	1.09	0.35	0.87	57.69	0.13	1.68	0.55
(KSSW)	0.87	39.5	0.92	1.89		0.56	30.59			

LOI-Loss on ignition

Kota Stone Slurry Waste

Kota stone slurry waste (KSSW) was used as a supplementary binder to partially replace fly ash, aiming to valorise stone-processing waste generated in large quantities by cutting and polishing units in Kota, Rajasthan, India. The slurry was collected in wet form, air-dried, oven-dried to remove residual moisture, and ground to obtain a fine powder suitable for geopolymer mortar applications. As summarized in Table 1, XRF analysis confirms that KSSW is predominantly calcium-rich, with high CaO content (39.5 wt.%) and moderate SiO_2 (30.59 wt.%), reflecting its limestone origin. The low alumina content indicates limited primary geopolymer reactivity; however, the fine particle size and carbonate-rich composition enable KSSW to act as an effective micro-filler and nucleation medium. In alkali-activated systems, the calcium contribution supports secondary reaction mechanisms and the formation of hybrid binding phases, contributing to improved matrix densification and early-age performance.

Natural Aggregates

Natural river sand sourced from the Banas River, Rajasthan, India, was used as the fine aggregate in geopolymer mortar preparation. The sand was clean, free from organic impurities, and brought to a saturated surface-dry (SSD) condition prior to mixing. Sieve analysis conducted in accordance with IS 383 and IS 2386 (Part I) [22,23] confirmed that the sand conformed to Zone III grading, ensuring suitable particle packing and consistency for mortar applications, as illustrated in Figure 3.

Design of Experiments

A Taguchi design of experiments (DoE) was employed to optimize the geopolymer mortar mixture and to quantify the combined influence of key processing parameters on ultrasonic pulse velocity (V_{UPV})

and water absorption, which are indicators of matrix compactness and durability, respectively. Five control factors were selected based on their established role in geo-polymerization and pore-structure development: binder replacement (B, %), NaOH molarity (M), alkalinity ratio ($R_{\frac{SS}{SH}}$), curing temperature (T), and alkaline solution-to-binder ratio ($R_{\frac{A}{B}}$). The selected factors and their levels are summarized in Table 2. The experimental domain comprised one six-level factor (B) and four three-level factors, resulting in 486 possible combinations (6×3^4). To reduce experimental effort while retaining statistical reliability, a mixed-level Taguchi L18 orthogonal array was adopted, which efficiently accommodates one multi-level factor along with multiple three-level factors while preserving orthogonality for main-effect analysis. In this framework, binder replacement denotes the percentage substitution of fly ash by Kota stone slurry waste. Each experimental run was prepared and tested under the specified conditions. Performance evaluation was carried out using the signal-to-noise (S/N) ratio, enabling robust identification of optimal factor levels by minimizing experimental variability.

For UPV, which reflects material compactness and internal continuity, the "larger-the-better" criterion was adopted:

$$\frac{S}{N} = -10\log_{10}\left(\frac{1}{n}\sum_{i=1}^{n}\frac{1}{y_i^2}\right) \quad (1)$$

For water absorption, which indicates pore connectivity and durability, the "smaller-the-better" criterion was used:

$$\frac{S}{N} = -10\log_{10}\left(\frac{1}{n}\sum_{i=1}^{n}y_i^2\right) \quad (2)$$

where y_i is the measured response value (UPV or water absorption) for the *i*th experiment, and *n* is the number of observations per trial.

Table 2. Factors and levels for Taguchi design

Factors		**Level1**	**Level 2**	**Level 3**	**Level 4**	**Level 5**	**Level 6**
Binder replacement%	B (%)	5	10	15	20	25	30
Molarity	M	10	12	14			
Alkalinity ratio	$R_{\frac{SS}{SH}}$	1	2	3			
Temperature	T	25	60	90			
Alkaline Solution to Binder Ratio	$R_{\frac{A}{B}}$	0.3	0.4	0.5			

The selection of control factors and their respective levels in the Taguchi orthogonal array was guided by an extensive review of existing literature, which consistently emphasizes the dominant role of alkaline activator chemistry and curing conditions in governing the performance of fly ash–based geopolymer mortars. Sodium hydroxide (NaOH) molarity is widely recognized as a critical parameter influencing geopolymerization kinetics, pore structure, compactness, and durability-related properties such as ultrasonic pulse velocity (UPV) and water absorption. Previous studies reported that moderate NaOH molarities promote effective dissolution of aluminosilicate species and lead to denser matrices, whereas excessively high molarities can induce rapid precipitation, increased porosity, and reduced performance [24,25]. Accordingly, NaOH molarity levels of 10 M, 12 M, and 14 M were selected to capture the optimum and post-optimum response range [26]. The sodium silicate–to–sodium hydroxide (SS/SH) ratio was incorporated due to its strong influence on silica availability, gel formation, and matrix densification, which directly affect UPV and water absorption. Literature reports indicate that optimized SS/SH ratios enhance the formation of compact aluminosilicate networks, while excessive silica may hinder polymerization and increase pore connectivity [27,28]. Therefore, SS/SH ratios of 1, 2, and 3 were adopted [29]. Curing temperature was selected as a key factor because it strongly controls reaction kinetics, microstructural evolution, and durability-related properties [30]. Elevated curing temperatures are known to accelerate geopolymerization and enhance matrix compactness, resulting in higher UPV and reduced water absorption; however, excessive temperatures may cause moisture loss and microcracking [31–33]. Thus, curing temperatures of 25 °C, 60 °C, and 90 °C were chosen to represent ambient, moderate, and elevated curing regimes. Finally, the alkaline activator-to-binder (A/B) ratio was included due to its direct influence on pore structure, workability, and permeability characteristics. Prior studies demonstrated that lower A/B ratios Favor matrix densification and reduced water absorption, whereas higher ratios increase pore volume despite improving workability [34,35]. Based on reported optimal ranges, A/B ratios of 0.3, 0.4, and 0.5 were selected [36,37].

Sample Preparation and Experimental Program

Geopolymer mortar specimens were prepared using Class F fly ash partially replaced with Kota stone slurry waste (KSSW), natural river sand as fine aggregate, and a blended alkaline activator consisting of sodium hydroxide (NaOH) and sodium silicate (Na_2SiO_3) (See Figure 4). NaOH solutions with molarities ranging from 10–14 M were prepared as per the Taguchi experimental matrix. Dry materials (binder and sand) were first mixed to achieve uniformity, followed by gradual addition of the pre-prepared alkaline activator and mixing water (See Figure 4). Mixing was carried out in a laboratory mixer until a homogeneous and workable mortar was obtained. Fresh mortar was cast into standard moulds and compacted immediately after mixing. After demoulding, specimens were cured under controlled temperatures of 25 °C, 60 °C, and 90 °C. Upon completion of curing, hardened specimens were evaluated for ultrasonic pulse velocity (UPV) to assess internal compactness and continuity, and water absorption to characterize pore structure and durability-related performance. The control mix was prepared using 100% fly ash with a binder-to-sand ratio of 1:3 and equal volumes of NaOH and Na_2SiO_3 (1:1).

Figure 4. Schematic illustration of material selection, mixing, casting, curing, and testing sequence.

RESULTS AND DISCUSSION

Design of Experiment

Based on the Taguchi signal-to-noise (S/N) analysis, the optimum level of each factor was identified from the maximum mean S/N ratio for ultrasonic pulse velocity (UPV) and the minimum mean S/N ratio for water absorption, as summarized in Table 3. For UPV, the binder replacement factor (B) exhibits its highest S/N value at Level 5 (72.23), corresponding to 25% replacement, which was therefore selected as the optimum. Similarly, NaOH molarity (M) attains its maximum S/N at Level 2 (71.94), indicating 12 M as the optimum molarity. The alkalinity ratio ($R_{\frac{SS}{SH}}$) shows its highest S/N value at Level 1 (71.87), leading to the selection of SS/SH = 1. For curing temperature (T), the maximum S/N value occurs at Level 2 (72.20), identifying 60 °C as the optimum curing condition. Finally, the alkaline solution-to-binder ratio ($R_{\frac{A}{B}}$) achieves its highest S/N at Level 3 (71.96), hence A/B = 0.5 was selected. For water absorption, which follows the "smaller-the-better" criterion, the minimum mean S/N values in Table 3 confirm the same optimum factor combination. The lowest water absorption corresponds to binder replacement at Level 5 (-16.50), molarity at Level 2 (-16.93), SS/SH at Level 1 (-16.81), curing temperature at Level 2 (-16.48), and A/B at Level 3 (-16.76). The consistency of optimum levels obtained from both UPV and water absorption responses demonstrates that the selected parameter combination simultaneously enhances matrix compactness (higher UPV) and durability (lower water absorption), validating the robustness of the Taguchi optimization. The Taguchi signal-to-noise (S/N) analysis using the "larger-the-better" criterion (Table 3) indicates that UPV is maximized at 25% binder replacement, 12 M NaOH, SS/SH = 1, curing at 60 °C, and A/B = 0.5.

Table 3. Response Table for Signal to Noise Ratios.

Factors	**Level**	**B (%)**	**M**	$R_{\frac{SS}{SH}}$	**T**	$R_{\frac{A}{B}}$
Ultrasonic Pulse Velocity	1	71.69	71.82	71.87	71.33	71.47
	2	71.54	71.94	71.71	72.20	71.75
	3	71.47	71.42	71.60	71.66	71.96
	4	71.62				
	5	72.23				
	6	71.82				
	$SN_{max.}$ -$SN_{min.}$	0.76	0.52	0.27	0.87	0.49
	Rank	2	3	5	1	4
Water Absorption	1	-17.85	-17.34	-16.81	-17.96	-18.18
	2	-17.71	-16.93	-17.32	-16.48	-17.68
	3	-18.50	-18.35	-18.49	-18.18	-16.76
	4	-17.09				
	5	-16.50				
	6	-17.59				
	$SN_{max.}$ -$SN_{min.}$	2.00	1.43	1.68	1.70	1.42
	Rank	1	4	3	2	5

The UPV and water-absorption results consistently indicate that the optimized KSSW-based geopolymer mortar achieved a markedly denser and less permeable matrix than the control mix. The control mortar recorded a UPV of 3754 m/s, whereas the optimized mix reached 4380 m/s, representing a ~16.7% increase in pulse velocity, which reflects improved internal continuity and reduced defect content (Figure 5). In parallel, water absorption decreased from 8.6% (control) to 3.1% (optimum), corresponding to a ~64.0% reduction, confirming substantial refinement of pore structure and moisture-ingress resistance (Figure 6). Across the L18 trials, UPV varied widely (3281.6–4326 m/s) while water absorption ranged from 10.5% down to 4.7%, and the optimum mix simultaneously achieved the best durability indicators (highest UPV and lowest absorption), evidencing the effectiveness of the selected factor window (Figure 5 & Figure 6). The inverse UPV–absorption trend is further supported by the fitted relationship (R^2 = 0.436), showing that mixes with higher UPV generally exhibit lower water absorption, validating UPV as a rapid, non-destructive proxy for compactness and transport resistance in these geopolymer mortars (Figure 7).

Enhancement in Mechanical Properties

After identifying the optimum mix through Taguchi optimization, confirmation specimens were cast and directly compared with the control (raw) mix to verify the effectiveness of the selected parameter combination. As illustrated in Figure 8 Improvement in compressive and flexural strength., the optimized geopolymer mortar exhibits a substantial enhancement in mechanical performance, with compressive strength increasing from 10.5 MPa to 25.6 MPa (≈143.8% improvement) and flexural strength increasing from 2.43 MPa to 3.95 MPa (≈62.6% improvement) due to more efficient geopolymerization, improved gel formation, denser microstructure, and stronger binder–aggregate interaction. This pronounced improvement confirms that the optimized combination promotes more efficient geopolymerization, leading to a denser and more homogeneous binder matrix capable of resisting both compressive loads and tensile stresses.

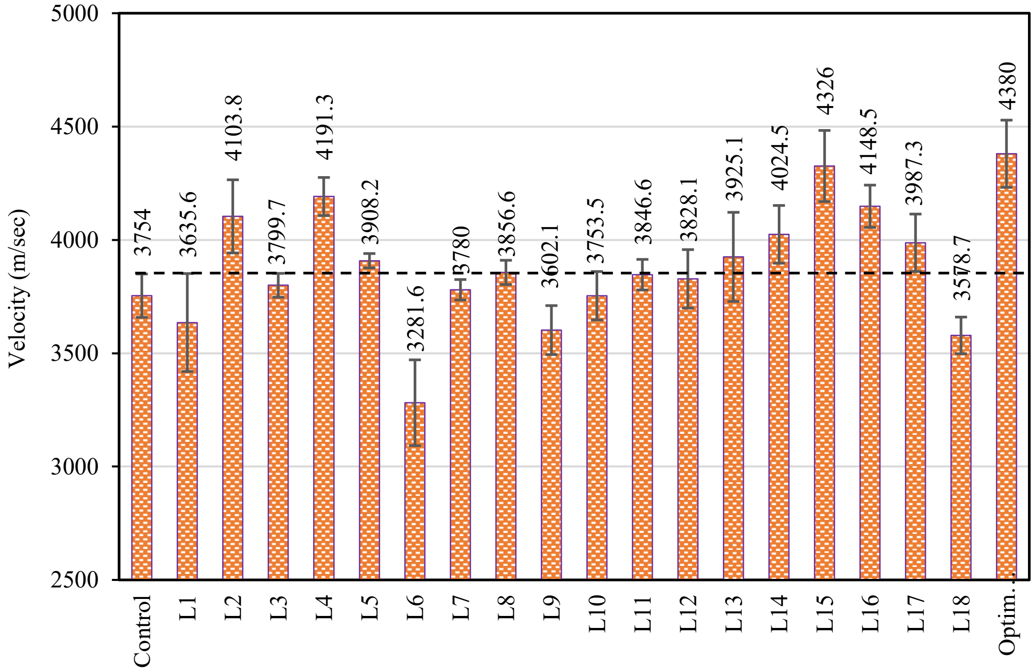

Figure 5. Comparison of ultrasonic pulse velocity (m/sec) test results.

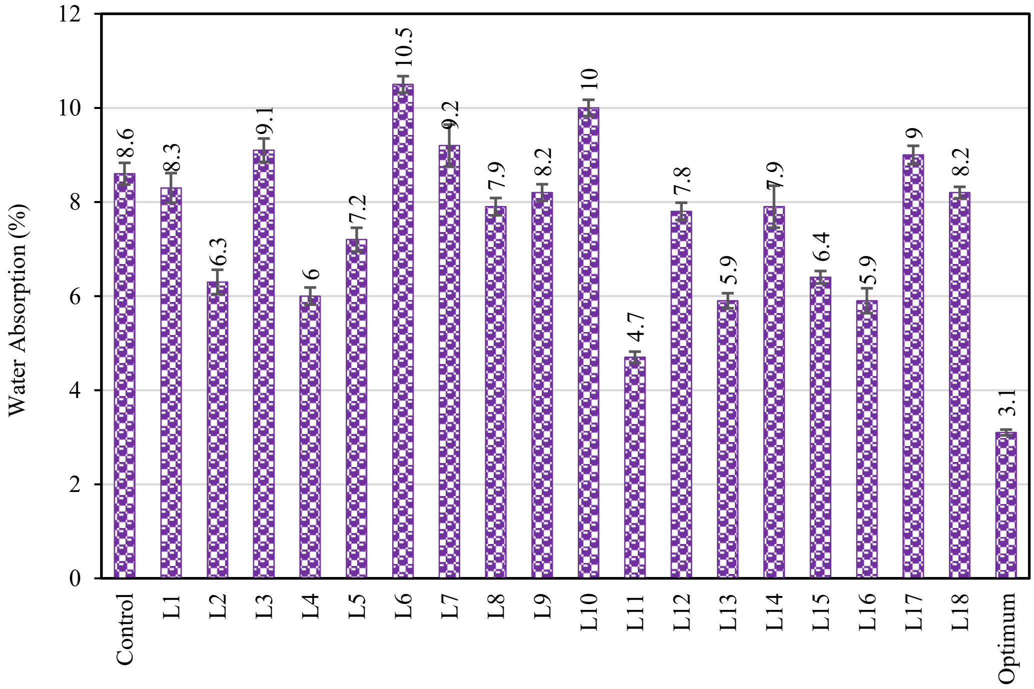

Figure 6. Comparison of water absorption test results.

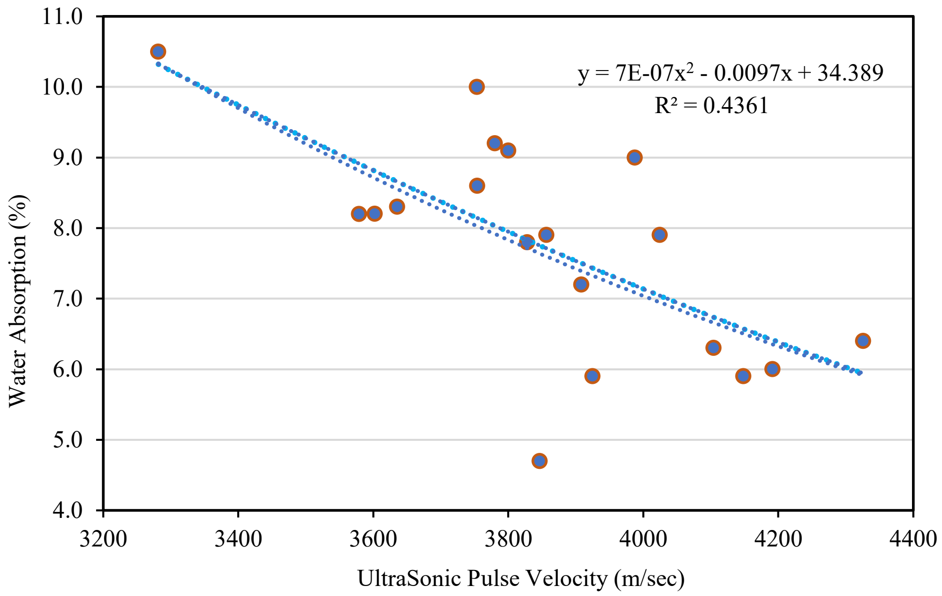

Figure 7. Relation between ultra sonic pulse velocity and Water Absorption.

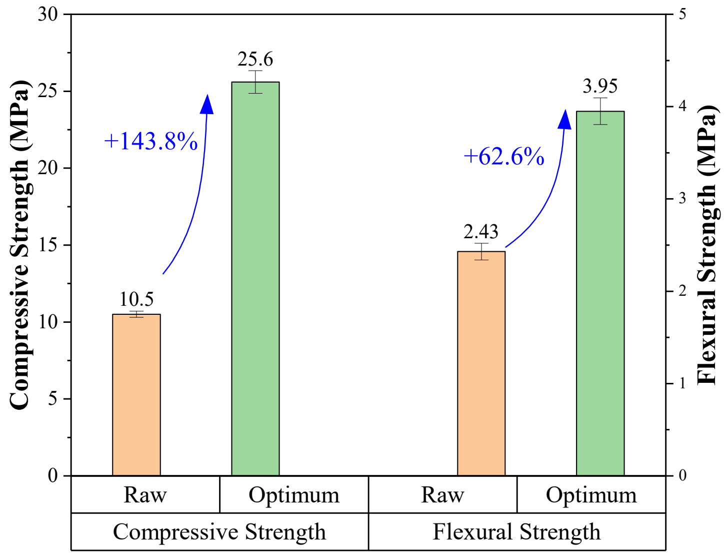

Figure 8. Improvement in compressive and flexural strength.

Regression Analysis

Nonlinear regression models were developed to quantify the influence of mix parameters on ultrasonic pulse velocity (V_{UPV}) and water absorption (W_a) of geopolymer mortar, based on the Taguchi experimental dataset. The proposed equations (Eqs. 3 and 4) incorporate linear, quadratic, and interaction terms of binder replacement (B), NaOH molarity (M), $R_{\frac{SS}{SH}}$ ratio, curing temperature (T), and alkaline solution-to-binder ratio ($R_{\frac{A}{B}}$), enabling robust prediction of durability-related performance indicators. For V_{UPV}, the regression model demonstrates excellent predictive capability, with an R^2 of 98.93% and adjusted R^2 of 95.45% (Table 4), indicating that the selected variables effectively explain variations in internal compactness. Positive coefficients associated with B, M, and T confirm their favorable role in enhancing matrix densification and wave propagation velocity, whereas the negative coefficient of $R_{\frac{A}{B}}$ reflects the adverse effect of excess activator on pore continuity. The significant quadratic term T^2 (35.83% contribution, $p < 0.001$) highlights the existence of an optimal curing temperature beyond which microcracking or moisture loss may reduce UPV. Interaction terms such as $M \times R_{\frac{A}{B}}$ and M×T were also statistically significant, demonstrating coupled effects between activator concentration and curing conditions.

Ultrasonic Pulse Velocity (m/sec)

$$V_{UPV} = 45 + 50 \times B + 407 \times M - 950 \times R_{\frac{SS}{SH}} + 49.15 \times T - 1353 \times R_{\frac{A}{B}} - 27.02 \times M^2 + 107.7 \times R^2_{\frac{SS}{SH}} - 0.4858 \times T^2 + 32.80 \times B \times R_{\frac{SS}{SH}} + 1.112 \times B \times T - 435 \times B \times R_{\frac{A}{B}} - 1.361 \times M \times T + 1002 \times M \times R_{\frac{A}{B}} \quad (3)$$

Water Absorption (%)

$$W_a = 34.1 - 1.185 \times B - 4.80 \times M - 2.53 \times R_{\frac{SS}{SH}} - 0.2368 \times T + 70.8 \times R_{\frac{A}{B}} + 0.2170 \times M^2 + 1.107 \times R^2_{\frac{SS}{SH}} + 0.001476 \times T^2 + 0.1001 \times B \times M + 0.00487 \times B \times T - 0.853 \times B \times R_{\frac{A}{B}} - 4.28 \times M \times R_{\frac{A}{B}} \quad (4)$$

Similarly, the water absorption model exhibits strong adequacy, with $R^2 = 95.32\%$ and adjusted $R^2 = 84.07\%$, confirming reliable prediction of permeability-related behavior. Negative coefficients for B, M, $R_{\frac{SS}{SH}}$, and T indicate reduced water uptake with increased binder substitution, optimized alkalinity, and elevated curing temperature, consistent with pore refinement mechanisms. In contrast, the large positive coefficient of $R_{\frac{A}{B}}$ confirms that excessive liquid content significantly increases water absorption by promoting capillary porosity. Quadratic and interaction terms particularly T2 (20.43% contribution) and B×T were statistically significant ($p < 0.05$), emphasizing the nonlinear dependency of moisture transport on curing regime and mix composition. The ANOVA results (Table 4) confirm the statistical significance ($p < 0.05$) of both regression models, with low prediction errors (PRESS) and acceptable information criteria (AICc and BIC), validating their suitability for durability-oriented optimization. Overall, the regression and ANOVA analyses demonstrate that UPV and water absorption can be reliably predicted and optimized using nonlinear Taguchi-based models, providing a robust framework for designing dense, low-permeability geopolymer mortars incorporating Kota stone slurry waste.

Table 4. Result of ANOVA for compressive strength

	S	**R-sq**	**R-sq(adj)**	**PRESS**	**R-sq(pred)**	**AICc**	**BIC**	**10-fold S**
UPV	53.5561	98.9%	95.45%	447537	58.25%	437.31	210.6	144.08
W_a	0.629114	95.3%	84.07%	32.8363	22.28%	179.34	51.81	1.3241
Ultrasonic Pulse Velocity (m/sec)	**Source**	**DF**	**Seq SS**	**Contribution**	**Adj SS**	**Adj MS**	**F-Value**	**P-Value**
	Regression	13	106054	98.93%	1060549	81581	28.44	0.003
	B	1	66957	6.25%	44174	44174	15.40	0.017
	M	1	86335	8.05%	14070	14070	4.91	0.091
	$R_{\frac{SS}{SH}}$	1	43740	4.08%	58077	58077	20.25	0.011
	T	1	71299	6.65%	179357	179357	62.53	0.001
	$R_{\frac{A}{B}}$	1	139651	13.03%	2123	2123	0.74	0.438
	M^2	1	71436	6.66%	38788	38788	13.52	0.021
	$R^2_{\frac{SS}{SH}}$	1	1173	0.11%	24926	24926	8.69	0.042
	T^2	1	384082	35.83%	507358	50735	176.8	0.000
	$B \times R_{\frac{SS}{SH}}$	1	3087	0.29%	76028	76028	26.51	0.007
	B×T	1	8011	0.75%	80271	80271	27.99	0.006

Journal of Polymer & Composites
Volume 14, Issue 3
ISSN: 2321-2810 (Online), ISSN: 2321-8525 (Print)

	S	R-sq	R-sq(adj)	PRESS	R-sq(pred)	AICc	BIC	10-fold S
	B× $R_{\frac{A}{B}}$	1	29627	2.76%	112979	11297	39.39	0.003
	M×T	1	1765	0.16%	22455	22455	7.83	0.049
	M× $R_{\frac{A}{B}}$	1	153385	14.31%	153385	15338	53.48	0.002
	Error	4	11473	1.07%	11473	2868		
Water Absorption	Regression	12	40.2705	95.32%	40.271	3.3559	8.48	0.014
	B	1	1.2652	2.99%	6.728	6.7280	17.00	0.009
	M	1	2.0008	4.74%	1.999	1.9985	5.05	0.075
	$R_{\frac{SS}{SH}}$	1	6.3075	14.93%	1.043	1.0427	2.63	0.165
	T	1	0.0018	0.00%	12.281	12.281	31.03	0.003
	$R_{\frac{A}{B}}$	1	3.9675	9.39%	6.112	6.1123	15.44	0.011
	M^2	1	2.5069	5.93%	2.528	2.5283	6.39	0.053
	SS/SH×SS/SH	1	0.6136	1.45%	3.248	3.2479	8.21	0.035
	T×T	1	8.6326	20.43%	6.289	6.2889	15.89	0.010
	B×M	1	3.2688	7.74%	10.517	10.516	26.57	0.004
	B×T	1	5.7211	13.54%	5.499	5.4991	13.89	0.014
	B× $R_{\frac{A}{B}}$	1	2.2944	5.43%	1.976	1.9765	4.99	0.076
	M× $R_{\frac{A}{B}}$	1	3.6902	8.73%	3.690	3.6902	9.32	0.028
	Error	5	1.9789	4.68%	1.979	0.3958		
	Total	17	42.2494	100.00%				

Validation of Regression Equation

A compares the experimentally measured and regression-predicted values of ultrasonic pulse velocity (V_{UPV}) and water absorption (W_a) for all 18 Taguchi trial mixes (Table 5). The results demonstrate a close agreement between experimental and predicted responses, confirming the robustness and predictive capability of the developed nonlinear regression models. For UPV, the percentage deviation between measured and predicted values remains low, generally within ±5%, with several mixes exhibiting errors below 2%. This indicates that the regression model effectively captures the combined effects of binder replacement, activator chemistry, and curing temperature on matrix densification and wave propagation characteristics. Similarly, the water absorption model shows good predictive accuracy, with most deviations below 6% and only a few mixes approaching ~10%, which is acceptable for durability-related properties. The slightly higher scatter in WA predictions compared to UPV is attributed to the greater sensitivity of water absorption to pore connectivity and microstructural heterogeneity. Overall, the low prediction errors across both responses confirm that the developed regression equations reliably describe the influence of mix parameters on internal quality and durability indicators of geopolymer mortar, making them suitable for performance prediction and mix optimization within the investigated domain (Table 5).

Table 5: *Comparison between experimental and regression-predicted compressive and flexural strength.*

Sample Cast	B%	M	$R_{\frac{SS}{SH}}$	Temp	$R_{\frac{A}{B}}$	V_{UPV} act	V_{UPV} Pred	Δv	W_a act	W_a Pred	Δw
L-1	5	10	1	25	0.3	3635.6	3656.18	0.24%	8.3	8.19	1.36%
L-2	5	12	2	60	0.4	4103.79	4099.12	1.94%	6.3	5.83	8.00%
L-3	5	14	3	90	0.5	3799.63	3832.44	2.81%	9.1	9.03	0.78%
L-4	10	10	1	60	0.4	4191.27	4176.22	1.31%	6	6.35	5.55%
L-5	10	12	2	90	0.5	3908.13	3904.86	5.00%	7.2	7.76	7.21%
L-6	10	14	3	25	0.3	3281.59	3274.66	2.15%	10.5	10.89	3.62%

Sample Cast	B%	M	$R_{\frac{SS}{SH}}$	Temp	$R_{\frac{A}{B}}$	V_{UPV} act	V_{UPV} Pred	Δ_V	W_a act	W_a Pred	Δ_W
L-7	15	10	2	25	0.5	3779.94	3750.68	5.50%	9.2	8.84	4.08%
L-8	15	12	3	60	0.3	3856.54	3848.22	7.28%	7.9	7.85	0.69%
L-9	15	14	1	90	0.4	3602.03	3581.64	0.03%	8.2	7.71	6.40%
L-10	20	10	3	90	0.4	3753.5	3752.32	4.01%	10	10.28	2.71%
L-11	20	12	1	25	0.5	3846.54	3910.15	3.16%	4.7	5.28	10.93%
L-12	20	14	2	60	0.3	3828.1	3873.66	5.21%	7.8	8.22	5.15%
L-13	25	10	2	90	0.3	3925.06	3937.02	3.36%	5.9	6.17	4.40%
L-14	25	12	3	25	0.4	4024.47	3997.65	1.58%	7.9	7.82	1.05%
L-15	25	14	1	60	0.5	4325.98	4299.66	3.19%	6.4	6.61	3.13%
L-16	30	10	3	60	0.5	4148.45	4177.92	1.07%	5.9	5.73	2.97%
L-17	30	12	1	90	0.3	3987.25	3987.16	4.97%	9	8.76	2.76%
L-18	30	14	2	25	0.4	3578.64	3578.66	0.23%	8.2	8.06	1.70%

Interaction Effect of Binder Replacement and NaOH Molarity

The combined effect of binder replacement (%) and NaOH molarity on the internal quality and durability of geopolymer mortar is illustrated through the 3D surface and contour plots for ultrasonic pulse velocity (UPV) and water absorption (Figure 9, Figure 10, Figure 11, & Figure 12). For UPV, an increase in molarity from 10 M to an intermediate range (≈12–13 M) results in a marked rise in pulse velocity across all binder replacement levels, indicating enhanced matrix densification due to improved dissolution of aluminosilicate species and formation of a compact geopolymeric gel network. However, at higher molarity (14 M), UPV decreases for several binder contents, suggesting microstructural discontinuities caused by excessive alkalinity and rapid reaction kinetics. The highest UPV values are consistently observed at intermediate binder replacement levels (≈20–25%) combined with moderate molarity, defining an optimum densification zone. A complementary trend is observed for water absorption, where absorption decreases with increasing molarity up to an optimum level and then increases at higher molarity, reflecting increased pore connectivity at excessive alkali concentrations (Figure 11, & Figure 12). Minimum water absorption occurs within the same binder–molarity window that yields maximum UPV, confirming that mixes with higher pulse velocity possess a denser and less permeable microstructure. The inverse relationship between UPV and water absorption is therefore reinforced by the interaction plots, demonstrating that optimal KSSW incorporation coupled with controlled alkalinity improves both internal compactness and durability performance of geopolymer mortar.

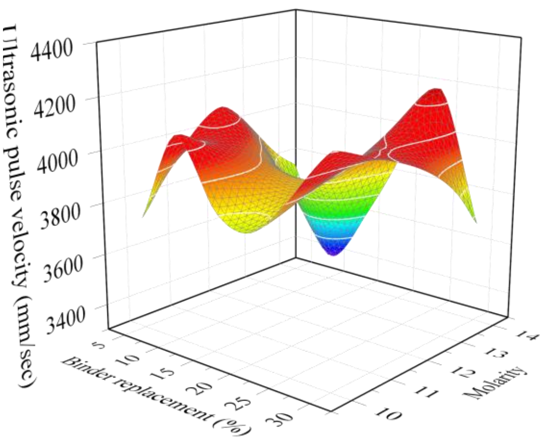

Figure 9. 3D surface plot showing the interaction effect of binder content and molarity for ultrasonic pulse velocity.

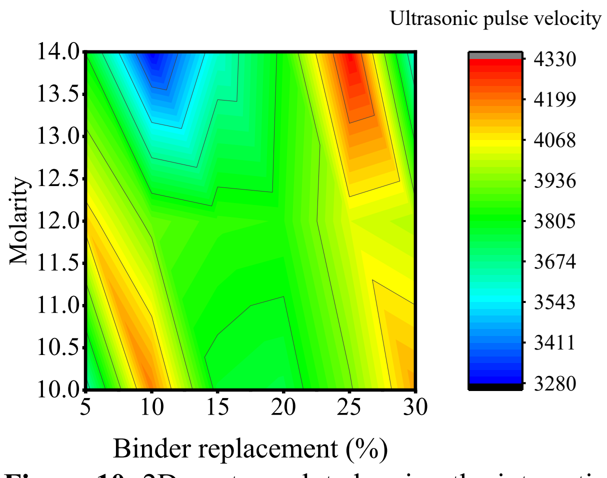

Figure 10. 2D contour plot showing the interaction effect of binder content and molarity for ultrasonic pulse velocity.

Journal of Polymer & Composites
Volume 14, Issue 3
ISSN: 2321-2810 (Online), ISSN: 2321-8525 (Print)

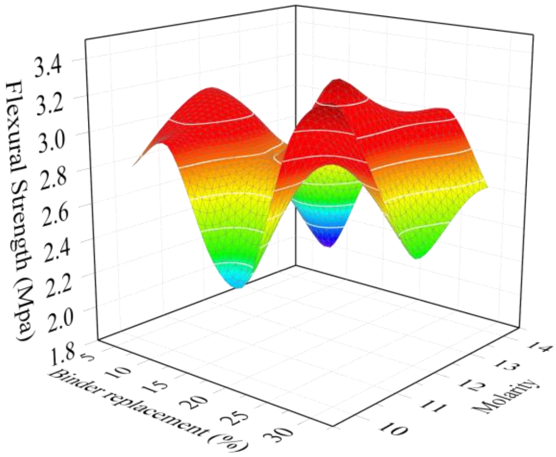

Figure 11. 3D surface plot showing the interaction effect of binder content and molarity for water absorption.sss

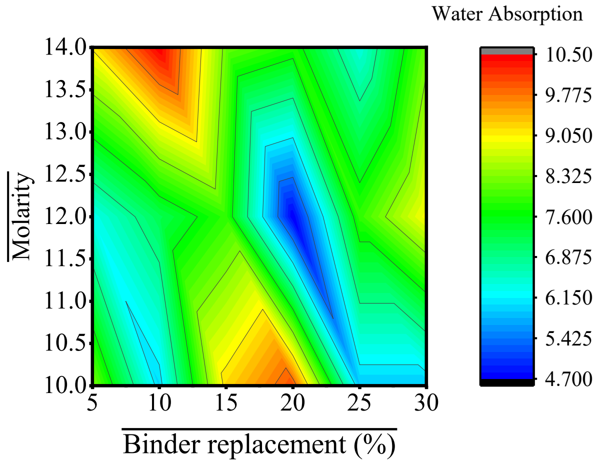

Figure 12. 2D contour plot showing the interaction effect of binder content and molarity for water absorption.

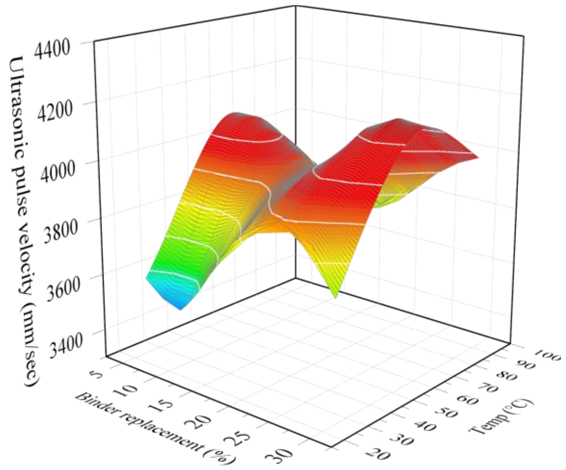

Figure 13. 3D surface plot showing the interaction effect of binder content and temperature for ultrasonic pulse velocity.

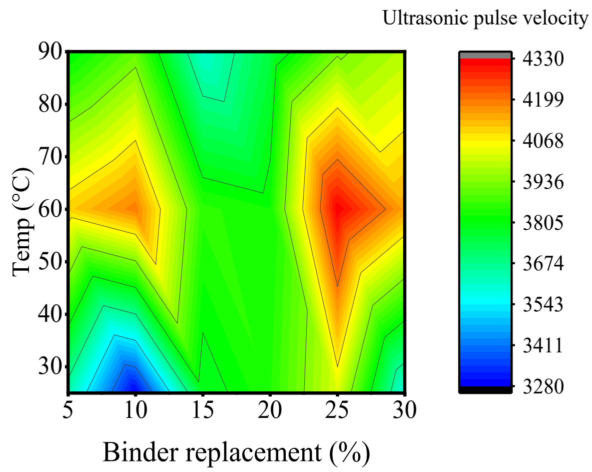

Figure 14. 2D contour plot showing the interaction effect of binder content and temperature for ultrasonic pulse velocity.

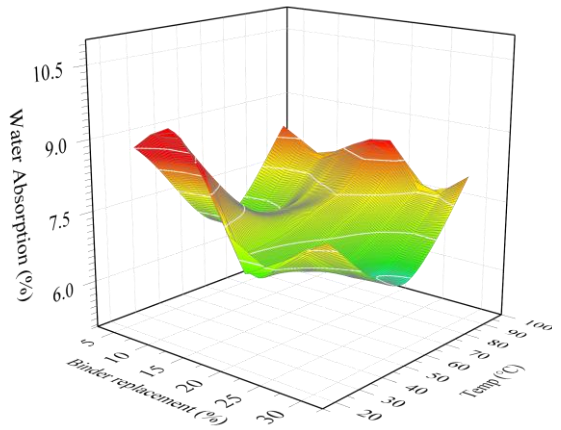

Figure 15. 3D surface plot showing the interaction effect of binder content and temperature for water absorption.

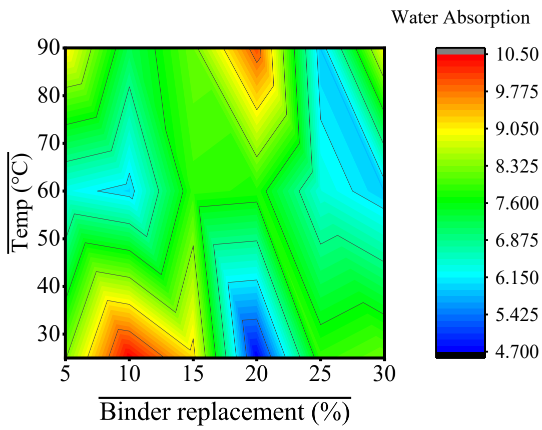

Figure 16. 2D contour plot showing the interaction effect of binder content and temperature for water.

Interaction Effect of Binder Replacement (%) and Curing Temperature

The coupled influence of binder replacement (%) and curing temperature on ultrasonic pulse velocity (UPV) and water absorption is illustrated by the 3D response surfaces and contour plots (Figure 13, Figure 14, Figure 15, & Figure 16). For UPV, increasing the curing temperature from ambient to moderate levels significantly enhances pulse velocity across most binder replacement ranges, reflecting improved geopolymerization kinetics, accelerated gel formation, and increased matrix compactness. However, at higher temperatures (≈90 °C), UPV gains diminish or decline for some mixes, particularly at low or excessive KSSW contents, likely due to rapid moisture loss and microstructural discontinuities. The contour plots indicate a clear optimum UPV zone at moderate curing temperature (~60 °C) combined with intermediate binder replacement (≈20–25%), where pulse velocity reaches the highest bands, signifying a dense and homogeneous microstructure. A complementary trend is observed for water absorption. Moderate thermal curing markedly reduces water absorption by promoting pore refinement and improved gel continuity, whereas excessive curing temperatures lead to localized increases in absorption, attributed to thermal shrinkage and microcrack formation. The lowest water absorption values are consistently concentrated within the same 20–25% binder replacement and ~60 °C curing window, confirming enhanced durability performance under these conditions. Overall, the interaction plots demonstrate that curing temperature and binder replacement act synergistically, and optimal durability and internal quality are achieved only when thermal activation is balanced with appropriate KSSW incorporation, avoiding under- or over-activation of the geopolymer matrix.

Comparison with previous studies

The mechanical performance of the optimized KSSW–fly ash geopolymer mortar with stone- and limestone-based waste mortars reported in the literature and with relevant codal provisions (Table 6). The optimized mix developed in this study (25% KSSW replacement) achieved 25.6 MPa compressive strength and 3.95 MPa flexural strength at 28 days, demonstrating performance comparable to or higher than several geopolymer and cement mortars incorporating dimensional-stone wastes. Compared with limestone-modified geopolymer systems, the present mortar significantly outperforms geopolymer mortar incorporating limestone powder with FA+BFS (16.16 MPa compressive and 2.88 MPa flexural strength), highlighting the effectiveness of KSSW combined with optimized alkaline activation and curing (Table 6) [38]. While higher strengths have been reported for calcium-rich geopolymer systems such as one-part lime-activated construction-and-demolition waste mortars and calcined dolomite powder geopolymer mortars (≈42 MPa compressive strength), these systems employ different precursor chemistries and activation mechanisms that inherently promote higher early strength [39,40]. Relative to cement-based mortars incorporating stone wastes, the optimized geopolymer mortar exhibits superior strength compared with ornamental stone processing waste cement mortar and comparable performance to stone dust–waste marble aggregate mortars, while remaining below high-strength marble powder–fly ash cement mortars [41–43].

Table 6. Comparison of present study with previous literature and international standards.

Source	Waste material	Binder system	Replacement level	Curing age	Compressive strength (MPa)	Flexural strength (MPa)
This Study	Kota Stone Slurry Waste (KSSW)	Fly ash–KSSW geopolymer mortar ($NaOH + Na_2SiO_3$ activator)	25% KSSW	28 days	25.6	3.95
(Aslan and Erkan 2024) [38]	Limestone powder (LP) (with FA + BFS)	Geopolymer mortar (FA + BFS + LP)	Mix No. 9: LP = 21.66% (binder blend)	28 days	16.16	2.88
(Moreira *et al*. 2022a) [41]	Ornamental stone processing waste (OSPW)	Cement mortar (CP V-ARI)	30% OSPW	28 days	12.56	3.12

(Woźniak *et al*. 2022) [42]	Stone dust + waste marble aggregate	Cement	10%	28 days	20.54	4.5
(Kogbara et al. 2024) [39]	Construction & demolition waste (CDW) (mineral waste stream)	One-part lime-activated geopolymer mortar	55%	28 days	42.0	5.8
(Youssf *et al*. 2025) [44]	Brick-and-stone cutting waste (BSCW)	Ambient-cured geopolymer mortar	25%	Ambient-cured;	32.76	-
(Shaaban *et al*. 2025) [40]	Calcined dolomite powder (CDP)	Geopolymer mortars	45%	28 Days	42.35	4.3
(Doğan and Demir 2021) [43]	Marble powder + fly ash (cement mortar)	Cement mortar (CEM I 42.5R)	20%	28 Days	49.5	9.5
(IS 2250 1981) [45]		Cement:sand mortar	1:3 corresponds to grade MM 7.5	28 days	≥ 7.5	
(ASTM C270 2025) [46]		Masonry mortar classification		28-day	Type M: 17.2 Type S: 12.4 Type N: 5.2 Type O: 2.4	

Importantly, from a codal perspective, both the control and optimized geopolymer mortars exceed the IS 2250 minimum strength requirement (≥ 7.5 MPa), and the optimized mix comfortably surpasses the compressive strength thresholds defined for masonry mortars under ASTM C270, confirming its suitability for structural masonry and repair applications [45,46].

CONCLUSIONS

This study optimized a Kota stone slurry waste (KSSW)–modified fly ash geopolymer mortar using a Taguchi-based experimental framework and validated performance through regression modelling, ANOVA, and non-destructive durability indicators. The principal conclusions are summarized as follows:

- The optimal geopolymer mortar composition was achieved at 25% KSSW replacement, 12 M NaOH, SS/SH = 1, curing at 60 °C, and A/B = 0.5, consistently identified as optimal across UPV and water absorption.
- The UPV increased from 3754 m/s (control) to 4380 m/s (optimum), corresponding to an improvement of approximately +16.7%, indicating significantly enhanced matrix densification.
- Water absorption decreased from 8.6% (control) to 3.1% (optimum), representing a substantial ~64% reduction, confirming refinement of pore structure and improved resistance to moisture ingress.
- The optimized mix achieved 25.6 MPa compressive strength and 3.95 MPa flexural strength at 28 days, reflecting increases of +143.8% in compression and +62.6% in flexure relative to the control mortar.
- Regression models incorporating linear, quadratic, and interaction terms accurately predicted UPV and water absorption, with ANOVA identifying curing temperature (T), NaOH molarity (M), and activator-to-binder ratio (A/B) as dominant contributors. Prediction errors remained within acceptable limits (<10%), confirming model robustness.
- Response surface analysis demonstrated that moderate alkalinity (≈12 M) combined with intermediate KSSW replacement (≈20–25%) and controlled thermal curing (≈60 °C) maximized UPV while minimizing water absorption, emphasizing the importance of balanced reaction kinetics and microstructural stability.

Overall, the findings demonstrate that KSSW can be effectively valorized as a supplementary binder in geopolymer mortar, enabling substantial improvements in strength, durability, and internal quality. The integration of statistical optimization with durability-oriented indicators provides a robust, resource-efficient pathway for sustainable geopolymer mortar design. Future research should focus on long-term durability, environmental exposure resistance, and life-cycle CO_2 assessment to support field-scale adoption and standardization.

AUTHOR CONTRIBUTIONS

All authors contributed to the development of manuscript.

FUNDING

This research received no specific grant from any funding agency in the public, commercial, or not-for-profit sectors.

Notations

The following symbols are used in this paper:

- $R_{\frac{A}{B}}$ – Alkaline solution-to-binder ratio
- Adj MS – Adjusted mean square (ANOVA)
- Adj SS – Adjusted sum of squares (ANOVA)
- AI – Artificial intelligence (only if used; otherwise delete)
- AICc – Corrected Akaike information criterion
- Al_2O_3 – Aluminium oxide
- ANOVA – Analysis of variance
- ASTM – ASTM International (formerly American Society for Testing and Materials)
- B% – Binder replacement / binder replacement percentage
- BFS – Blast furnace slag (as used in literature comparison table)
- BIC – Bayesian information criterion
- BSCW – Brick-and-stone cutting waste
- BR – Binder replacement (remove if you already use B or B%)
- $CaCO_3$ – Calcium carbonate (calcite)
- $CaMg(CO_3)_2$ – Dolomite
- CaO – Calcium oxide
- C–A–S–H – Calcium–alumino–silicate–hydrate
- C–S–H – Calcium–silicate–hydrate
- CI – Crystallinity index
- CO_2 – Carbon dioxide
- CP V-ARI – Portland cement type CP V-ARI (Brazilian designation, as in cited literature)
- CPWD – Central Public Works Department (India)
- Cu–Kα – Copper K-alpha radiation
- CDP – Calcined dolomite powder
- CDW – Construction and demolition waste
- DF – Degrees of freedom
- DOE – Design of experiments
- FA – Fly ash
- GGBFS – Ground granulated blast furnace slag
- GP – Geopolymer
- IS – Indian Standard
- KBr – Potassium bromide
- KSSW – Kota stone slurry waste
- LP – Limestone powder

- M – Molarity (NaOH concentration, mol/L)
- MS – Mean square (ANOVA)
- Na_2SiO_3 – Sodium silicate
- NaOH – Sodium hydroxide
- N–A–S–H – Sodium–alumino–silicate–hydrate gel
- C-(N)-A–S–H – Calcium-(sodium)-alumino–silicate–hydrate (hybrid gel)
- OPC – Ordinary Portland cement
- OSPW – Ornamental stone processing waste
- Q – Quartz
- R^2 – Coefficient of determination
- R^2(adj) – Adjusted coefficient of determination
- R^2(pred) – Predicted coefficient of determination
- S – Standard deviation of regression (model "S")
- Seq SS – Sequential sum of squares (ANOVA)
- SH – Sodium hydroxide solution
- S/N – Signal-to-noise ratio (Taguchi)
- SS – Sodium silicate solution
- $R_{\frac{SS}{SH}}$ – Sodium silicate to sodium hydroxide ratio
- T – Curing temperature
- 2θ – Diffraction angle

DATA AVAILABILITY STATEMENT

Data will be available on request.

ACKNOWLEDGEMENT

The authors gratefully acknowledge the support of the Department of Metallurgy, Malaviya National Institute of Technology (MNIT) Jaipur, for providing the facilities for XRD testing, and the MREC Centre, MNIT Jaipur, for facilitating the FTIR analysis required for this study.

REFERENCE

1. Ricciotti L, Frettoloso C, Franchino R, Pisacane N, Aversa R. Geopolymer Materials: Cutting-Edge Solutions for Sustainable Design Building. Sustainability (Switzerland) 2025;17. https://doi.org/10.3390/SU17167483.
2. Zhang P, Zheng Y, Wang K, Zhang J. A review on properties of fresh and hardened geopolymer mortar. Compos B Eng 2018;152:79–95. https://doi.org/10.1016/J.COMPOSITESB.2018.06.031.
3. Zhang X, Li J, Yu Y, Wang H. Investigating the water vapor sorption behavior of bamboo with two sorption models. J Mater Sci 2018;53:8241–9. https://doi.org/10.1007/S10853-018-2166-Y.
4. Wang J, Zhu L, Wan D, Xue Y. Research Progress and Trend Analysis of Solid Waste Resource Utilization in Geopolymer Concrete. Buildings 2025;15. https://doi.org/10.3390/BUILDINGS15183370.
5. Fahim Huseien G, Mirza J, Ismail M, Ghoshal SK, Abdulameer Hussein A. Geopolymer mortars as sustainable repair material: A comprehensive review. Renewable and Sustainable Energy Reviews 2017;80:54–74. https://doi.org/10.1016/J.RSER.2017.05.076.
6. Alhawat M, Ashour A, Yildirim G, Aldemir A, Sahmaran M. Properties of geopolymers sourced from construction and demolition waste: A review. Journal of Building Engineering 2022;50. https://doi.org/10.1016/J.JOBE.2022.104104.
7. Naresh T, Mallik M, Venkateswara Rao S, Dubey S. Performance and microstructural optimization of sustainable geopolymer mortars using fly ash, ground granulated blast furnace slag, and rice husk ash. Structural Concrete 2025. https://doi.org/10.1002/SUCO.70192.

8. Boakye K, Khorami M. Impact of Low-Reactivity Calcined Clay on the Performance of Fly Ash-Based Geopolymer Mortar. Sustainability (Switzerland) 2023;15. https://doi.org/10.3390/SU151813556.
9. Herbudiman B, Subari S, Nugraha B, Pratiwi I, Rinovian A, Widyaningsih E, et al. Effect of Different Ceramic Waste Powder on Characteristics of Fly Ash-Based Geopolymer. Civil Engineering Journal (Iran) 2024;10:431–43. https://doi.org/10.28991/CEJ-2024-010-02-06.
10. Ebrahim A allah M, Ahmed DA, Abu-Elwafa R. Development of an eco-friendly geopolymer mortar using slag and fly ash with high bentonite content for thermal and environmental applications. Sci Rep 2024;14. https://doi.org/10.1038/S41598-024-76780-5.
11. Samuvel Raj R, Prince Arulraj G, Anand N, Kanagaraj B, Lubloy E, Naser MZ. Nanomaterials in geopolymer composites: A review. Developments in the Built Environment 2023;13. https://doi.org/10.1016/J.DIBE.2022.100114.
12. Zerihun B. Nano-metakaolin-enhanced fly ash and cement-based geopolymer mortar. Journal of Material and Process Technologies 2024;1:23–7. https://doi.org/10.69660/JMPT.V1I1.62.
13. Biricik H, Kırgız MS, Galdino AG de S, Kenai S, Mirza J, Kinuthia J, et al. Activation of slag through a combination of NaOH/NaS alkali for transforming it into geopolymer slag binder mortar – assessment the effects of two different Blaine fines and three different curing conditions. Journal of Materials Research and Technology 2021;14:1569–84. https://doi.org/10.1016/J.JMRT.2021.07.014.
14. Felaous K, Aziz A, Achab M, Fernández-Raga M, Benzaouak A. Optimizing Alkaline Activation of Natural Volcanic Pozzolan for Eco-Friendly Materials Production: An Investigation of NaOH Molarity and Na2SiO3-to-NaOH Ratio. Sustainability (Switzerland) 2023;15. https://doi.org/10.3390/SU15054453.
15. Salim MU, Moro C. Towards sustainable construction: Performance evaluation of slag-cenosphere geopolymers under different NaOH concentrations. Journal of Building Engineering 2024;91. https://doi.org/10.1016/J.JOBE.2024.109605.
16. Guo L, Liu J, Zhou M, An S. Effect of an alkali activators on the compressive strength and reaction mechanism of coal gangue-slag-fly ash geopolymer grouting materials. Constr Build Mater 2024;426. https://doi.org/10.1016/J.CONBUILDMAT.2024.136012.
17. Çelikten S, Sarıdemir M, Soloğlu M. Effects of elevated temperatures and cooling regimes on the waste andesite dust-based geopolymer mortars. Constr Build Mater 2024;422. https://doi.org/10.1016/J.CONBUILDMAT.2024.135857.
18. Karaaslan C, Şek Ş, Turan C. Utilising High-Ambient-Temperature Curing in the Development of Low-Calcium Geopolymers. Buildings 2025;15. https://doi.org/10.3390/BUILDINGS15162974.
19. Usman Kankia M, Baloo L, Danlami N, Zawawi NA, Bello A, Muhammad SI. Microstructural Analysis and Compressive Strength of Fly Ash and Petroleum Sludge Ash Geopolymer Mortar under High Temperatures. Sustainability (Switzerland) 2023;15. https://doi.org/10.3390/SU15129846.
20. Strzałkowski P, Król R, Kawalec W, Sówka I, Czajka KM. Characteristics of Waste Generated in Dimension Stone Processing. Energies 2021, Vol 14, Page 7232 2021;14:7232. https://doi.org/10.3390/EN14217232.
21. Jalalian MH, Bagherpour R, Khoshouei M. Wastes production in dimension stones industry: resources, factors, and solutions to reduce them. Environ Earth Sci 2021;80:1–13. https://doi.org/10.1007/S12665-021-09890-2/METRICS.
22. IS 383. Coarse and Fine Aggregate for Concrete - Specification. Bureau of Indian Standards 1970. https://law.resource.org/pub/in/bis/S03/is.383.1970.pdf (accessed May 4, 2025).
23. IS 2386-7. Methods of Test for Aggregates for Concrete, Part VII: Alkali Aggregate Reactivity. Bureau of Indian Standards 1963. https://law.resource.org/pub/in/bis/S03/is.2386.7.1963.pdf (accessed July 10, 2024).
24. Mariamah, Chairunnisa N, Nurwidayati R. The Effect of Natrium Hydroxide Molarity Variation and Alkali Ratio on the Compressive Strength of Geopolymer Paste and Mortar. IOP Conf Ser Earth Environ Sci 2023;1184. https://doi.org/10.1088/1755-1315/1184/1/012025.

25. Wardhono A, Risdianto Y, Sabariman B, Hidajati NW. The role of NaOH molarity on the strength performance of geopolymer mortar prepared by a combination of fly ash, rice husk ash, and kaolin at heat-cured condition. IOP Conf Ser Earth Environ Sci 2024;1416:012044. https://doi.org/10.1088/1755-1315/1416/1/012044.
26. Sunarsih ES, As'ad S, Mohd. Sam AR, Kristiawan SA. The effect of sodium hydroxide molarity on setting time, workability, and compressive strength of fly ash-slag-based geopolymer mortar. J Phys Conf Ser 2023;2556. https://doi.org/10.1088/1742-6596/2556/1/012019.
27. Enoh MKE, Ushie DO. Effect of Sodium Silicate to Hydroxide Ratio and Sodium Hydroxide Concentration on the Physico-Mechanical Properties of Geopolymer Binders. East African Journal of Engineering 2023;6:113–21. https://doi.org/10.37284/EAJE.6.1.1361.
28. Chenafi MH, Makhloufi Z, Bekkai AO, Berkak H. Enhancing the performance of sustainable geopolymers: Insights into liquid-to-solid and alkali ratios. Research on Engineering Structures and Materials 2025. https://doi.org/10.17515/RESM2025-635MA0122RS.
29. Jeeva Chithambaram S, Sanjay Kumar, Prasad MM. Study on effect of sodium hydroxide concentration on geopolymer mortar. Lecture Notes in Civil Engineering 2019;25:651–8. https://doi.org/10.1007/978-981-13-3317-0_58.
30. Bhina MR, Liu KY, Hu JEHY, Tsai CT. Investigation of the Mechanical Properties of Quick-Strength Geopolymer Material Considering Preheated-to-Room Temperature Ratio of Sand, Na2SiO3-to-NaOH Ratio, and Fly Ash-to-GGBS Ratio. Polymers (Basel) 2023;15. https://doi.org/10.3390/POLYM15051084.
31. Öz HÖ, Doğan-Sağlamtimur N, Bilgil A, Tamer A, Günaydin K. Process development of fly ash-based geopolymer mortars in view of the mechanical characteristics. Materials 2021;14. https://doi.org/10.3390/MA14112935.
32. Zhang Z, Huo Z, Yang Z, Wang X, Xia J. Curing Condition and NaOH Concentration on the Mechanical Properties of Fly Ash Based Geopolymer Mortars. International Journal of Sustainable Construction Engineering and Technology 2023;14:279–86. https://doi.org/10.30880/IJSCET.2023.14.01.025.
33. Syavanka LN, Herwani H, Faisal F. Effect of Curing Temperature on Mechanical Properties of Fly Ash-Based Geopolymer Concrete from Bengkayang Power Plant. Jurnal Teknik Sipil 2025;25:1748–58. https://doi.org/10.26418/JTS.V25I1.88504.
34. Sunarsih ES, As'ad S, Mohd.Sam AR, Kristiawan S. The Effect of Alkali Activator to Binder Ratio on Workability, Density, and Compressive Strength of Fly Ash-Slag Based Geopolymer Mortar. Nano Hybrids and Composites 2024;45:121–7. https://doi.org/10.4028/P-MFE2JS.
35. GholamReza Ahmadi. Shrinkage and Mechanical Resistance of Steel Fiber Reinforced Geopolymer Mortars Containing Industrial By-Product GGBS; Solution to Binder Affect in Oven Curing Condition. Power System Technology 2024;48:1274–90. https://doi.org/10.52783/PST.942.
36. Khaleel Sk, Reddy DrLS. Enhancement of Mechanical Properties of Geopolymer Ferrocement through Incorporation of a Novel Binder and through Optimization of Alkaline Activator Ratios. South East Eur J Public Health 2024:1081–8. https://doi.org/10.70135/SEEJPH.VI.1971.
37. Saeki Y, Fujikake K, Sasatani T, Kuwahara N, Kuroiwa D. Development of Cast-in-Place FA-GGBFS-Based Geopolymer Mortar: An Experimental Study. Practice Periodical on Structural Design and Construction 2022;27. https://doi.org/10.1061/(ASCE)SC.1943-5576.0000681.
38. Aslan S, Erkan İH. The Effects of Fly Ash, Blast Furnace Slag, and Limestone Powder on the Physical and Mechanical Properties of Geopolymer Mortar. Applied Sciences 2024, Vol 14, 2024;14. https://doi.org/10.3390/APP14020553.
39. Kogbara RB, Al-Zubi A, Mortada Y, Hammoud A, Masad EA, Khraisheh MK. Lime-activated one-part geopolymer mortars from construction, demolition and industrial wastes. Results in Engineering 2024;21:101739. https://doi.org/10.1016/J.RINENG.2023.101739.
40. Shaaban M, Hussien OF, Khalifa S. Characteristics and Microstructure of Geopolymer Mortars incorporating Ground Granulated Blast Furnace Slag and Calcined Dolomite Powder: A

Sustainable Solution for Construction Materials. Engineering, Technology & Applied Science Research 2025;15:21791–9. https://doi.org/10.48084/ETASR.10095.

41. Moreira PI, de Oliveira Dias J, de Castro Xavier G, Vieira CM, Alexandre J, Monteiro SN, et al. Ornamental Stone Processing Waste Incorporated in the Production of Mortars: Technological Influence and Environmental Performance Analysis. Sustainability (Switzerland) 2022;14. https://doi.org/10.3390/SU14105904/S1.
42. Woźniak ZZ, Chajec A, Sadowski Ł, Woźniak ZZ, Chajec A, Sadowski Ł. Effect of the Partial Replacement of Cement with Waste Granite Powder on the Properties of Fresh and Hardened Mortars for Masonry Applications. Materials 2022, Vol 15, 2022;15. https://doi.org/10.3390/MA15249066.
43. Doğan C, Demir İ. The Effect of Marble Powder and Fly Ash on Mechanical Properties of Cement Mortars. Afyon Kocatepe Üniversitesi Fen Ve Mühendislik Bilimleri Dergisi 2021;21:1137–45. https://doi.org/10.35414/AKUFEMUBID.977280.
44. Youssf O, Eldin DS, Tahwia AM, Youssf O, Eldin DS, Tahwia AM. Eco-Friendly High-Strength Geopolymer Mortar from Construction and Demolition Wastes. Infrastructures 2025, Vol 10, 2025;10. https://doi.org/10.3390/INFRASTRUCTURES10040076.
45. IS 2250. Code of Practice for Preparation and Use of Masonry Mortars : Bureau of Indian Standards. 1981. https://doi.org/https://law.resource.org/pub/in/bis/S03/is.2250.1981.pdf.
46. ASTM C270. Specification for Mortar for Unit Masonry. West Conshohocken, PA: ASTM International; 2025. https://doi.org/10.1520/C0270-25A.

